Supplemental information to:

Operando EXAFS reveals role of oxygen in oxide-derived silver catalysts for electrochemical CO_2 reduction

Authors: Nienke. J. Firet[1], Marijn A. Blommaert[1], Anirudh Venugopal[1], Thomas Burdyny[1], Divya Bohra[1], Alessandro Longo*[2,3], Wilson. A. Smith*[1]

(1) Materials for Energy Conversion and Storage (MECS), Department of Chemical Engineering, Faculty of Applied Sciences, Delft University of Technology, van der Maasweg 9, 2629 HZ Delft, The Netherlands
(2) Netherlands Organization for Scientific Research (NWO), The European Synchrotron Radiation Facility (ESRF), CS40220, 38043 Grenoble Cedex 9, France
(3) ISMN-CNR, UOS Palermo, Via Ugo La Malfa, 153, 90146 Palermo, Italy

Experimental section

Sample fabrication

Ag foils (Mateck, 99.9%, 0.25 mm) and Ti foils (Alfa Aesar, 99.5%, annealed, 0.25 mm) sputtered with 600 nm of silver were treated with potential pulses in a homemade Teflon 2-compartment cell, separated by a Nafion membrane. Both compartments were filled with 0.2 M NaOH (99.9% purity, Boom chemicals). A Pt thin film was used as counter electrode, a glass Redrod electrode (1 M KNO_3, XR440, Radiometer Analytical) was used as reference electrode. The sample fabrication was performed by cycling between 0 and 1.2 V vs. Ag/AgCl at 50 Hz for 5 hours.

Material characterization

SEM images were collected on a JEOL JSM-6010LA SEM microscope with a tungsten hairpin filament. Images were collected at an accelerating voltage of 10 kV and a working distance of 10 mm. GIXRD patterns (20°−116.5° 2θ) were collected using a Bruker D8 Discover X-ray diffractometer in Grazing incidence mode with a copper source (λ = 1.5418 Å), Göbel mirror and 0.2° Soller slit. XRD patterns (25°−100° 2θ) were collected using a Bruker D8 Advance X-ray diffractometer in Bragg−Brentano configuration with a cobalt source (λ = 1.7889 Å). XPS experiments were conducted using a Thermo Scientific K-alpha apparatus equipped with an

Al K-alpha X-ray Source and a Flood Gun to avoid charging of the sample. Parameters used for the measurements were: spot size of 400 µm, pass energy of 50 eV, energy step size of 0.1 eV, dwell time of 50 ms, 10 scans in the vicinity of the Ag 3d and O1s orbital binding energy.

Electrochemical characterization

Gaseous products from CO_2 reduction were measured on an online Compact GC (Compact GC 4.0 from Global Analytical Solutions with H2/O2/C1-C5 analyser). The GC took an aliquot every three minutes. CO_2 reduction was performed for one hour at a fixed potential of -0.8 V vs. RHE. The reported faradaic efficiencies are averaged values of at least two samples. The reaction was performed in a homemade PMMA 2-compartment cell. Both compartments were filled with CO_2-satureated 0.1 M $KHCO_3$ (99.995% K_2CO_3 from Sigma Aldrich). A Pt thin film was used as counter electrode, a glass Ag/AgCl electrode (saturated KCl, XR300, Radiometer Analytical) was used as reference electrode. A Nafion membrane separated the two compartments, 11.5 ml/min of CO_2 was continuously bubbled through both compartments. The solvent resistance (R_u) was between 30 and 35 Ω in the experiments.

Electrochemical surface areas were measured through the double layer capacitance method. CVs were taken over a non-Faradaic region (0.51 to 0.61 V vs RHE) in nitrogen saturated 0.1 M $NaClO_4$ at different scan rates (10, 30, 50, 60, 70, 90 and 100 mV/sec). The non-Faradaic region was determined by taking the open circuit value of reduced Ag as the value around which the CV scan was performed. The slope of the total geometric current versus the scan rate gave the capacitance which was used to determine the relative roughness by normalizing the capacitance of the Ag foil.

DFT calculations

A 2x3x6 slab size was used for Ag(110). The Ag metal slab and surfaces with and without adsorbed intermediates were created using the Atomic Simulation Environment (ASE).[1] All density functional theory (DFT) calculations were carried out with the projector augmented wave (PAW) method as implemented in the GPAW software.[2,3] BEEF-vdW exchange correlation (xc) functional was used to perform all the energy calculations[4,5] with plane-wave (PW) cutoff energy value of 450 eV. Lattice constants for the bulk FCC metal were calculated using the same xc functional and PW cutoff for a residual force on all atoms of less than 0.005 eV $Å^{-1}$. The resulting lattice constant for Ag, 4.1384 Å, was used for all other energy calculations.

For the geometry optimization, the top two metal layers as well as the adsorbed atoms were allowed to relax until a residual force of less than 0.01 eV $Å^{-1}$ is reached. The self-consistent field (SCF) convergence criterion was set to 5 x 10^{-4} eV for adsorption energy calculations. A 12 Å vacuum layer was placed above the periodically repeating slabs. The Fermi-Dirac method was used to smear the Fermi level with an electronic temperature of 0.1 eV and a

Pulay mixing of the resulting electronic density was applied. A (3x3x1) k-point sampling was used and a grid spacing between 0.16 Å and 0.2 Å was used for all calculations.

XAS characterization

X-ray absorption spectra were recorded at the Dutch-Belgian beamline (DUBBLE, 26A) of the European Synchrotron Radiation Facility (ESRF) in Grenoble, France. Silver K-edge (25515.59 eV) spectra were recorded between 25300 and 26055 eV. The energy of the X-ray beam was tuned by a double-crystal monochromator operating in fixed-exit mode using a Si(111) crystal pair. XANES and EXAFS spectra of the samples were collected in fluorescence mode using a 9-element Ge detector (Ortec Inc.), whereas reference spectra of the metallic Ag foil and the silver oxides were collected in transmission mode using Ar/He-filled ionization chambers at ambient temperature and pressure. The photon flux of incoming X-rays is ~2.5 * 10^{10} photons/cm^2. Ex situ samples were measured at grazing incidence angles of 0°, 0.1°, 5° and 10° degrees. In operando samples were measured at 6° degrees. EXAFS data analysis was performed on data that was averaged from at least 3 20 minute scans.

For the operando measurements a home-made electrochemical flow cell (Figure S5) was used. The electrolyte was pulled through the cell volume using a peristaltic pump operated at 40 rpm. The cell had a silver catalyst as WE, a coiled Pt wire as counter electrode and a 2 mm diameter PEEK Leakless Ag/AgCl RE (ET072, EDAQ). The electrolyte was CO_2 saturated 0.1 M $KHCO_3$. The headspace of the electrolyte reservoir was purged with CO_2 during measurements to ensure constant CO_2 saturation and avoid bubbles in the incoming electrolyte. A Biologic SP240 potentiostat was used to control the potential in a three-electrode configuration. The Ag and ODAg samples were all used for 1 hour of CO_2 reduction coupled to the GC prior to their measurements in the XAS cell. This way, the ODAg state was already reached before the sample was measured using XAS.

EXAFS data analysis

Because of the cell design, measurements could not be performed in transmission geometry. Instead, the EXAFS spectra were acquired in fluorescence mode under different angles of incidence. Spectra of non-dilute samples that were measured in fluorescence mode need to be corrected with a self-absorption correction, for instance using the Athena software. We used a transmission EXAFS spectrum of a 5 µm thick pure silver foil to derive the typical coordination number obtained for similar samples. By comparing our self-absorption corrected fluorescence spectra with the transmission spectrum of pure silver we were able to get good estimations for the size of the required corrections. In short, the operando spectra needed a correction of a 0° degree in and 90° degree out configuration (Athena software, Fluorescence self-absorption correction option) due to the combination of a thick substrate, low angle of incidence and shielding by the cell. The ex situ samples were not shielded by a cell and therefore only required a mild 45 degree correction. The sputtered samples could by

analysed without any correction since the thin 600 nm sputtered layer falls within the limit of thin samples that do not require a self-absorption correction.

After the correction, the EXAFS data is fitted using Viper software. Since the measurements are performed at room temperature, the higher shells are relatively noisy. We therefore only fit the spectra up to ~ 3 to 4 Å from the absorber atom. For a silver metal, this corresponds to only the first shell, for the silver oxides, the first (Ag-O) and the second (Ag-Ag) shell can be fitted. The k-range is taken from 2.5 to 10 $Å^{-1}$, all Fourier transforms are k^2-weighted. In some cases the error in fitting the coordination number could not be properly estimated by the software. In these cases instead the difference between the normalised and the normalised + smoothed data was taken as the error.

Ag-O model clusters

An fcc cuboctahedral cluster was modelled to calculate a core-shell structure with a metal silver core and a silver oxide shell.[6] the metal cluster was varied in size by adding additional A-Ag shells. The calculations were performed on 2, 3 and 4 Ag-Ag shell cluster, all surrounded by one Ag-O shell. The coordination number of Ag-O for each Ag atom in the cluster was calculated and average over the entire cluster to yield the final Ag-O coordination numbers.

Applied potential during operando EXAFS measurements

A typical CO_2 reduction reaction at an ODAg catalyst is performed at -0.8 V vs. RHE. Hydrogen and CO are formed at this potential at a total current density of around 2 mA/cm^2. When we performed CO_2R at these potentials we generated bubbles that would stick to the catalyst surface. These bubbles strongly interfere with the EXAFS spectra: one spectrum takes roughly 20 minutes to record, if the amount of bubbles grows in this period of time (which will happen inevitably), the background signal of the EXAFS spectra will shift. This renders the spectrum useless for FT transformation or further data fitting. Therefore we could only generate proper EXAFS spectra by measuring operando at a very low overpotential. We measured at 0 and at -0.12 V vs. RHE. For comparison, an EXAFS spectrum obtained at -0.4 V vs. RHE is shown in Figure S1. When we normalise this spectrum and compare it to the Ag and ODAg used for fitting in the paper, we see how the main feature (the bump at 2 Å) remains the same between the two ODAg measured at different potentials. The signal at 1 Å that is only seen in the -0.4 V vs RHE spectrum most likely stems from noise since even strongly bound O in AgO displays the O-Ag bond at higher values of ~1.5 Å (Figure 5).

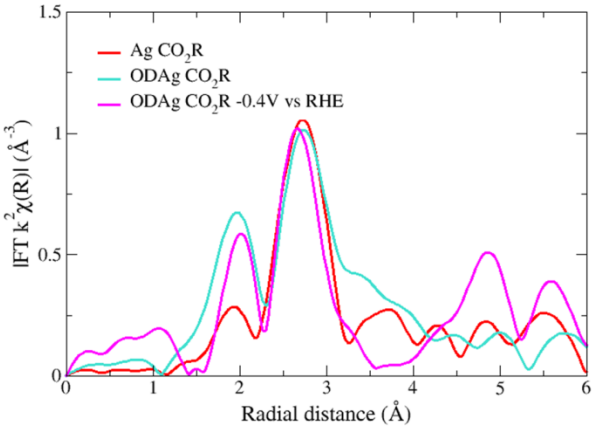

Figure S1. EXAFS spectra as shown in Figure 8 together with an ODAg catalyst measured at a higher overpotential to show the minor difference between measuring at 0 and at -0.4 V vs RHE for the fitted region (1.5 – 3.2 Å).

X-ray absorption fine structure spectroscopy theory

The data we obtain in a XANES/EXAFS measurement is the absorption coefficient μ of the photo-electron of the element of interest as a measure of energy. The energy range of the incoming X-rays is chosen to coincide with the orbital to be probed. In the case of the K-edge of silver (the Ag 1s orbital), this energy range is 25300 – 26055 eV, the absorption edge is at 25515.59 eV. To analyse XANES data (the first 50-80 eV above the absorption edge), the sample data is compared to reference samples of known composition and structure, in our case a pure silver foil and silver(I) and silver(II) oxide powders. The EXAFS is the 80 – 1000 eV above the edge and its function χ(E) is defined as equation 1. To analyse the EXAFS data, the energy is converted to the wavenumber k of the photo electron, as defined in equation 2.

$$\chi(E) = \frac{\mu(E) - \mu_0(E)}{\Delta\mu_0(E)} \qquad 1$$

$$k = \sqrt{\frac{2m(E - E_0)}{\hbar^2}} \qquad 2$$

In these equations, μ(E) is the measured absorption coefficient and μ_0(E) is the theoretical absorption coefficient for one isolated atom. $\Delta\mu_0$ is the adsorption edge jump, so the difference in μ between the pre-edge and the absorption. Wavenumber k is a function of the mass of an electron (m) and the absorption edge energy E_0.

The EXAFS equation (equation 3) can be modelled to the data χ (k) and is in fact a summation of these different frequencies that all have their own interatomic distance (R), coordination number (N) (a measure of the amount) and Debye Waller factor (σ) (the strain).

$$\chi(k) = \sum_i \frac{N_i f_i(k) e^{-2k^2\sigma_i^2}}{kR_i^2} \sin[2kR_i + \delta_i(k)] \qquad 3$$

The scattering amplitude f and the phase-shift δ are calculated according to the FEFF9 code[7] and can be used to fit the data to equation 3 by using R, N and σ as free parameters. Since the oscillations diminish quickly at larger distances from the absorber atom, χ (k) can be multiplied with a factor k^2 or k^3. For a pure metal, the different oscillations are the different shells around the absorber atom: silver atoms at various distances within the same unit cell. For an oxide, some shells are Ag-O contributions and others are Ag-Ag. The Fourier Transform (FT) of χ(k) gives a spectrum that is easier to interpret by eye compared to the χ(k) spectrum. The x-axis now displays the distance between the absorber atom and the neighbouring shells, the y-axis is a measure of the intensity.

Chronoamperometry and Faradaic efficiency over time

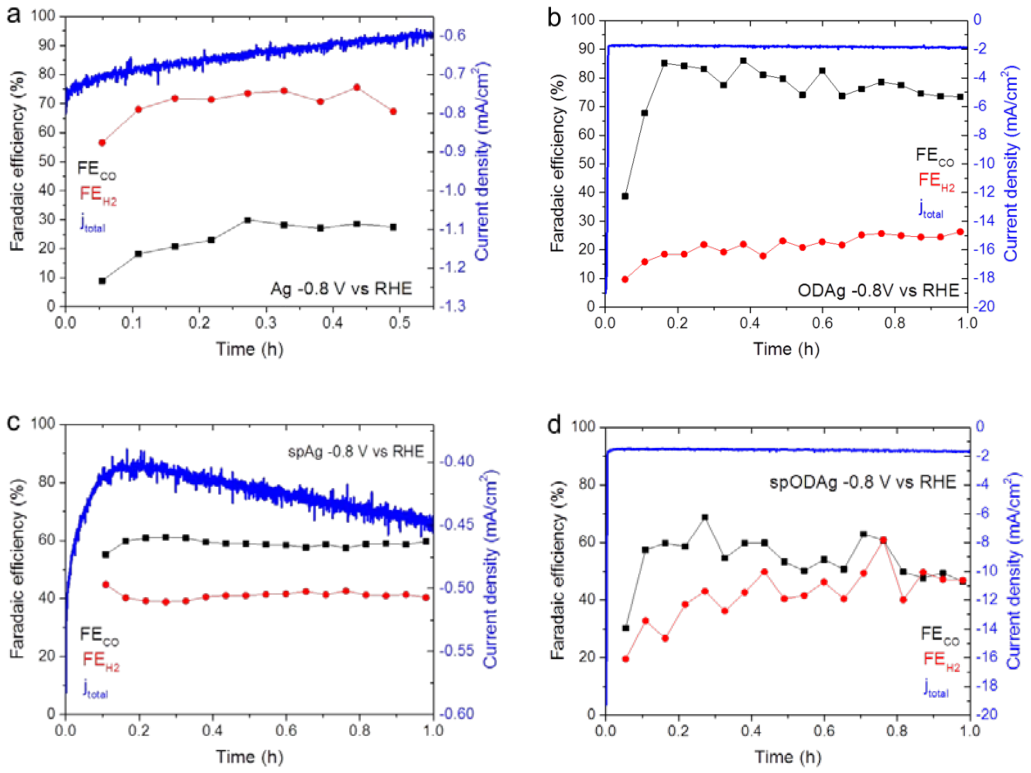

Figure S2. Current density and faradaic efficiency of carbon monoxide and hydrogen recorded for one hour at -0.8V vs RHE for (a) silver, (b) oxide-derived silver, (c) sputtered silver and (d) oxide-derived silver from a sputtered silver substrate.

XRD patterns

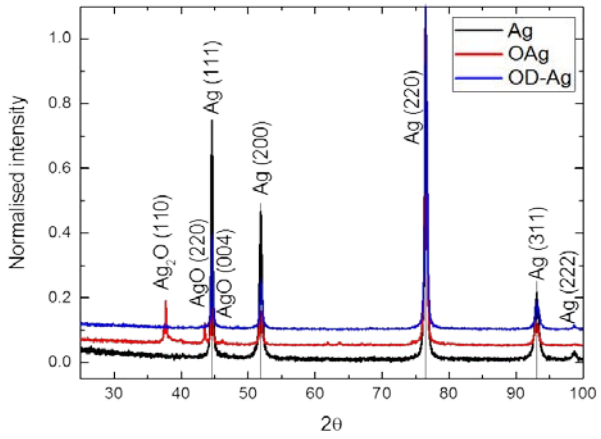

Figure S3. XRD patterns measured in Bragg-Brentano configuration of Ag, AgO_x and ODAg, showing the Ag_2O and AgO XRD reflections in the AgO_x sample. NB the XRD instrument was equipped with a cobalt source, resulting in a different 2θ pattern compared to the GIXRD patterns.

EXAFS cell design

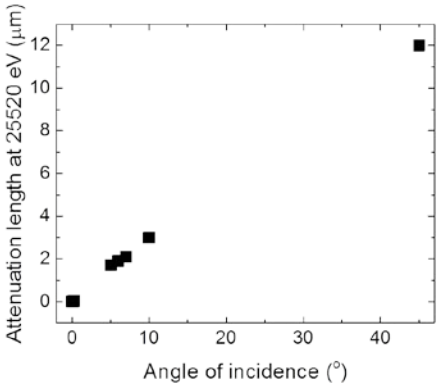

Angle of incidence (°)	Attenuation length
0	1.8 nm
0.1	3.2 nm
0.2	43 nm
5	1.7 μm
6	1.9 μm
7	2.1 μm
10	3 μm
45	12 μm

Figure S4. The attenuation length at the silver K-edge as a function of the X-ray beam incidence angle. The attenuation length is the depth into the probed material (normal to the surface) where the intensity has dropped to 1/e of its value at the surface (calculated without water layer). The adjacent table contains the values used in the graph.

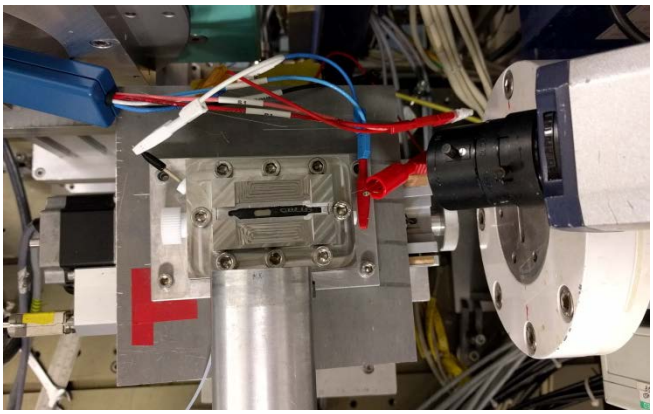

Figure S5. Top view picture of the experimental set-up used for in operando EXAFS data collection. X-ray source is on the left, fluorescence detector on the bottom of the picture.

$k^2\chi(k)$ and first derivative of μ(E)

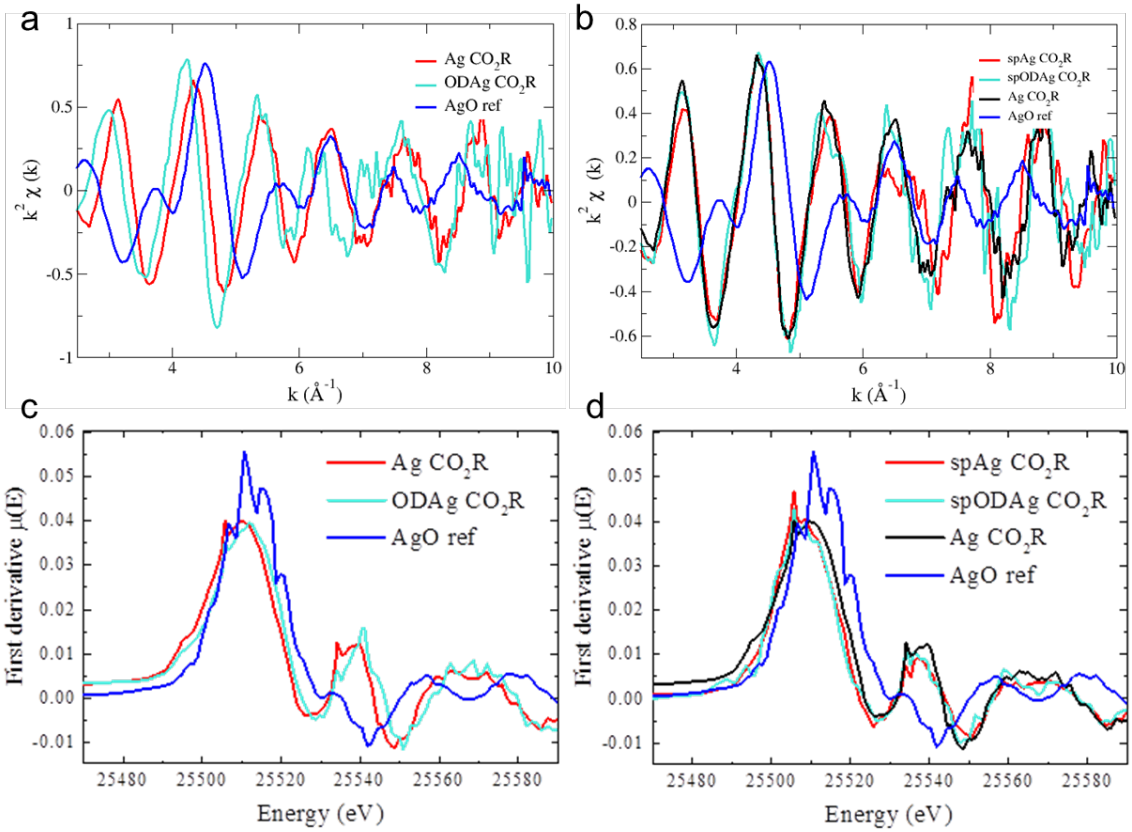

Figure S6. The $k^2\chi(k)$ spectra and first derivative of μ(E) of the data presented in Figure 4b and c. (a) and (c) silver and oxide-derived silver measured in operando are shown together with silver oxide reference to show the distinct difference in $k^2\chi(k)$ between Ag and ODAg in the lower frequency part of the spectrum. (b) and (d) sputtered silver and oxide-derived silver from a sputtered silver substrate are shown with reference to silver and silver oxide. The difference between the sputtered silver samples and pure silver is less strong.

Ex situ characterization of sputtered samples

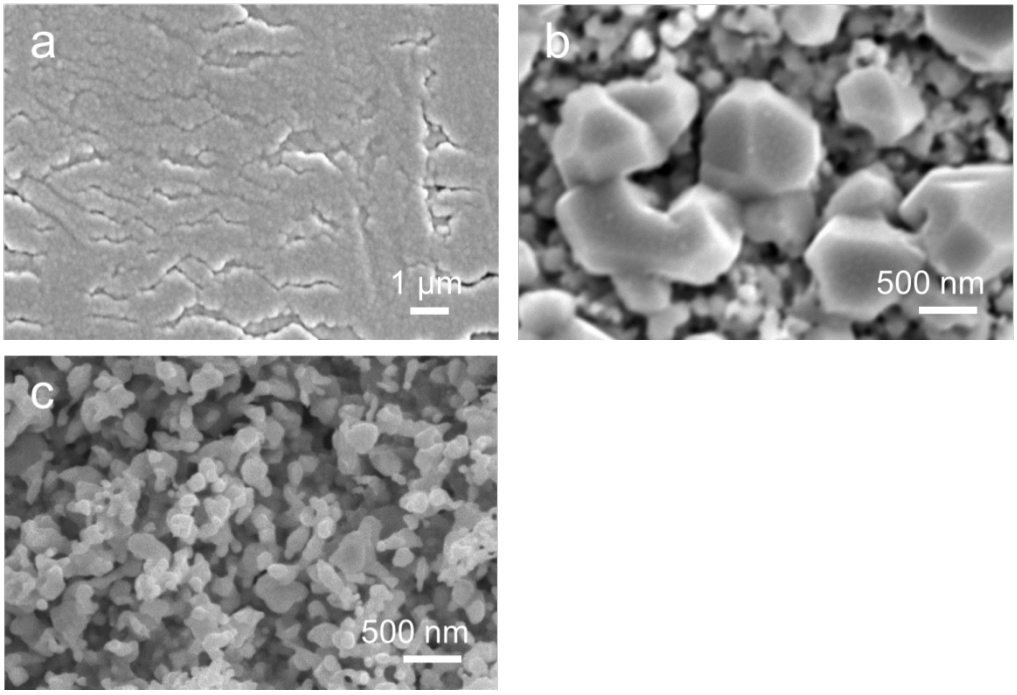

Figure S7. SEM images of sputtered samples: (a) untreated Ag on Ti foil substrate, (b) spAgO_x and (c) spODAg

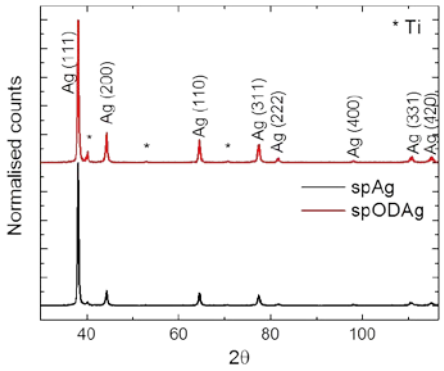

Figure S8. GIXRD patterns of sputtered Ag and oxide-derived silver from a sputtered silver substrate. Titanium reflections denoted by *.

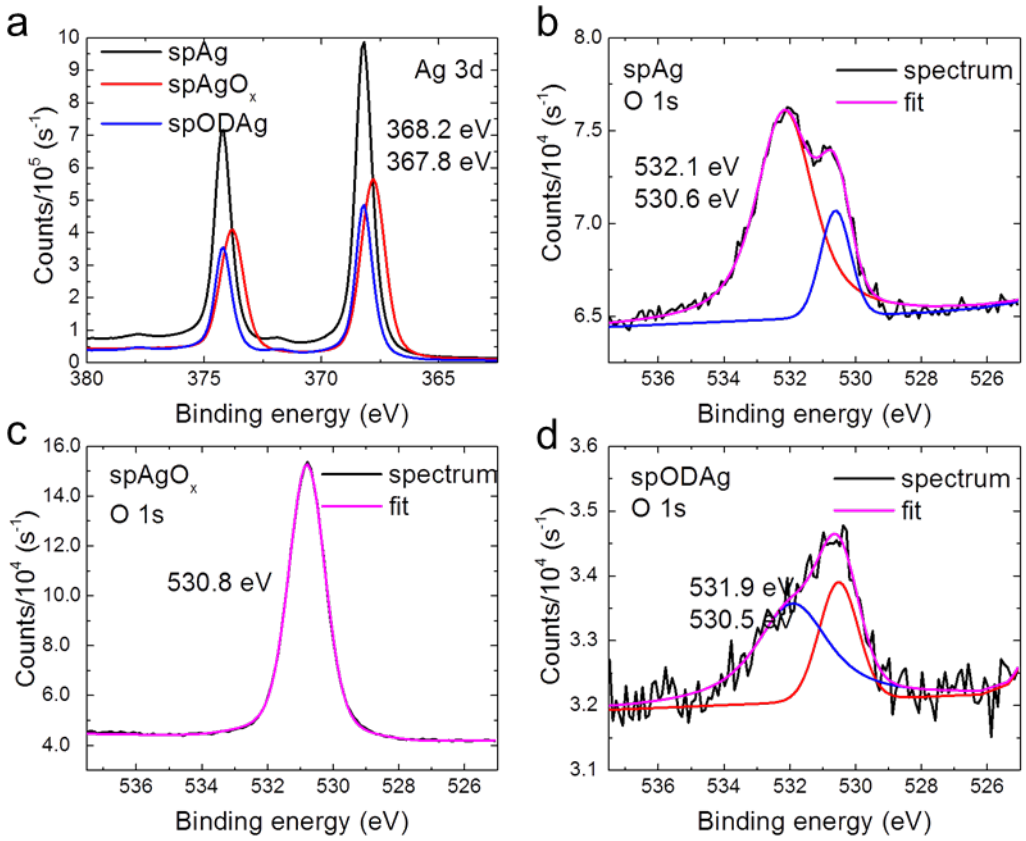

Figure S9. (a) Ag 3d XPS spectra of spAg, spAgO$_x$ and spODAg. The spAgO$_x$ precursor is not metallic but an oxide, as can be concluded from the shift in the Ag 3d peak. O 1s spectrum and fit of (b) spAg, (c) spAgO$_x$ and (d) spODAg, the red and blue lines indicate the deconvoluted peaks.

References

1. Bahn, S. R. & Jacobsen, K. W. An object-oriented scripting interface to a legacy electronic structure code. *Comput. Sci. Eng.* **4,** 56–66 (2002).
2. Enkovaara, J. *et al.* Electronic structure calculations with GPAW: A real-space implementation of the projector augmented-wave method. *J. Phys. Condens. Matter* **22,** 253202 (2010).
3. Mortensen, J. J., Hansen, L. B. & Jacobsen, K. W. Real-space grid implementation of the projector augmented wave method. *Phys. Rev. B* **71,** 35109 (2005).
4. Wellendorff, J. *et al.* Density functionals for surface science: Exchange-correlation model development with Bayesian error estimation. *Phys. Rev. B* **85,** 235149(23) (2012).
5. Wellendorff, J. *et al.* A benchmark database for adsorption bond energies to transition metal surfaces and comparison to selected DFT functionals. *Surf. Sci.* **640,** 36–44 (2015).
6. Longo, A. & Martorana, A. Distorted f.c.c. arrangement of gold nanoclusters: A model of spherical particles with microstrains and stacking faults. *J. Appl. Crystallogr.* **41,** 446–455 (2008).
7. Rehr, J. J., Kas, J. J., Vila, F. D., Prange, M. P. & Jorissen, K. Parameter-free calculations of X-ray spectra with FEFF9. *Phys. Chem. Chem. Phys.* **12,** 5503–5513 (2010).